Electrochimica Acta 574 (2026) 149342

Contents lists available at ScienceDirect

Electrochimica Acta

journal homepage: www.journals.elsevier.com/electrochimica-acta

Solubility-driven interfacial impedance in NCM523/graphite cells with sulfonate and sulfate lithium salts

Koji Abe [a,b,*], Keitatsu Miura [a], Yanko Marinov Todorov [b], Masaki Deguchi [c]

[a] Graduate School of Sciences and Technology for Innovation, Yamaguchi University, 2-16-1 Tokiwadai, Ube, Yamaguchi 755-8611, Japan
[b] Organization for Research Initiatives, Yamaguchi University, 2-16-1 Tokiwadai, Ube, Yamaguchi 755-8611, Japan
[c] Energy Research and Development Center, Panasonic Energy Co., Ltd., 1-1 Matsushita-cho, Moriguchi, Osaka 570-8511, Japan

ARTICLE INFO

Keywords:
Lithium-ion batteries
Lithium salt additives
Solubility
Charge-transfer resistance
Cathode electrolyte interphase (CEI)

ABSTRACT

Lithium-ion batteries using $LiNi_{0.5}Co_{0.2}Mn_{0.3}O_2$/graphite electrodes were investigated to clarify the effect of lithium sulfonate and sulfate electrolyte additives on interfacial impedance evolution. Electrochemical impedance spectroscopy, voltammetry, scanning electron microscopy, and X-ray photoelectron spectroscopy (XPS) were employed to analyze interfacial changes after cycling. Additives with intermediate solubility (0.5–2 wt%), particularly CH_3OSO_3Li, most effectively suppressed impedance growth compared with both sparingly and highly soluble salts. Total cell impedance decreased by up to 30% after 300 cycles relative to a vinylene carbonate-containing baseline electrolyte, while maintaining comparable capacity retention. Cyclic voltammetry showed no distinct redox features attributable to additive decomposition, indicating negligible electrochemical decomposition. XPS detected sulfur-containing interphase species at both electrodes without measurable changes in apparent interphase thickness. These results suggest that impedance suppression is associated with additive solubility and interfacial composition. The findings provide practical insight into electrolyte design for controlling interfacial impedance.

1. Introduction

Lithium-ion batteries (LIBs) are widely used in portable electronics and electric vehicles (EVs), where energy density and internal impedance are key performance factors. Control of the interfacial impedance at the electrode/electrolyte interface is important because reduction of internal resistance is required to shorten charging times in LIBs [1,2].

In 1999, we proposed the concept of a “functional electrolyte,” in which a small amount of an additive is introduced to regulate the electrode/electrolyte interfacial structure through preferential interfacial reactions [3,4]. This approach enables modification of interfacial properties without altering electrode materials, requiring only adjustment of the electrolyte composition [5–7]. In the present study, this concept serves as a general framework for interpreting additive-driven interfacial effects.

Conventional additives such as vinylene carbonate (VC) form a solid electrolyte interphase (SEI) on graphite through reductive decomposition [8–10], while cathode electrolyte interphases (CEIs) are generally formed via oxidative decomposition and interfacial coordination processes [11–13]. However, the CEI is typically thinner and more difficult to characterize than the SEI, and its formation mechanisms remain less clearly understood.

In addition to sacrificial decomposition-type additives, sulfur-containing lithium salts, such as sulfonates and sulfates, have been reported to influence interfacial behavior and impedance evolution [14]. For example, lithium fluorosulfonate (FSO_3Li) has been shown to reduce charge-transfer resistance in $LiFePO_4$/graphite cells, although its effect has been associated with electrochemical decomposition processes [15]. In contrast, our previous studies suggested that lithium methanesulfonate-derived species could be detected on electrode surfaces after cycling [16], indicating possible interfacial involvement in the absence of clear evidence of distinct electrochemical decomposition.

Although sulfur-containing lithium salts have been widely studied as electrolyte additives, a systematic comparison of solubility-dependent impedance behavior under practical full-cell conditions has not been reported. The role of solubility as a design parameter also remains unclear, particularly with respect to whether effective impedance suppression requires sacrificial electrochemical decomposition or whether

* Corresponding author at: Graduate School of Sciences and Technology for Innovation, Yamaguchi University, 2-16-1 Tokiwadai, Ube, Yamaguchi 755-8611, Japan.
E-mail address: abekoji@yamaguchi-u.ac.jp (K. Abe).

https://doi.org/10.1016/j.electacta.2026.149342
Received 1 May 2026; Received in revised form 8 June 2026; Accepted 14 June 2026
Available online 15 June 2026
0013-4686/© 2026 The Author(s). Published by Elsevier Ltd. This is an open access article under the CC BY license (http://creativecommons.org/licenses/by/4.0/).

other interfacial processes may contribute under practical operating conditions.

In this study, lithium salts containing sulfonate and sulfate functional groups were comparatively investigated in NCM523/graphite pouch cells. The selected additives include sparingly soluble lithium methanesulfonate (CH_3SO_3Li), moderately soluble sulfate-based salts such as lithium methanesulfate (CH_3OSO_3Li) and lithium ethanesulfate ($C_2H_5OSO_3Li$), and highly soluble sulfonate salts including lithium trifluoromethanesulfonate (CF_3SO_3Li) and lithium fluorosulfonate (FSO_3Li). Through this comparative approach, the possible relationship between additive solubility and impedance evolution was examined using electrochemical and surface analytical techniques under practical cycling conditions.

2. Experimental

2.1. Chemical materials

The electrolyte consisting of 1 M $LiPF_6$ in ethylene carbonate (EC)/dimethyl carbonate (DMC) (1:2 by volume; $\leq$10 ppm H_2O and $\leq$30 ppm HF) was supplied by MU Ionic Solutions Co., Ltd. (Japan). Vinylene carbonate (VC), DMC, lithium methanesulfate (CH_3OSO_3Li), lithium ethanesulfate ($C_2H_5OSO_3Li$), and lithium fluorosulfonate (FSO_3Li) were also purchased from MU Ionic Solutions Co., Ltd. (Japan). Lithium methanesulfonate (CH_3SO_3Li) was obtained from Kanto Denka Kogyo Co., Ltd. (Japan), and lithium trifluoromethanesulfonate (CF_3SO_3Li) was purchased from FUJIFILM Wako Pure Chemical Co., Ltd. (Japan).

2.2. Electrode materials

The positive and negative electrodes are hereafter referred to as the cathode and anode, respectively. The electrode sheets were fabricated according to a previously reported procedure [16].

The cathode consisted of $LiNi_{0.5}Co_{0.2}Mn_{0.3}O_2$ (NCM523) as the active material and was coated onto aluminum (Al) foil using a mixture of NCM523, acetylene black (AB), and polyvinylidene fluoride (PVdF) at a weight ratio of 92:5:3. The areal loading was 9.5 mg cm^{-2}, and the electrode density after pressing was 2.5 g cm^{-3}. The thickness of the cathode active material layer was approximately 38 μm.

The anode consisted of natural graphite (NG) as the active material and was coated onto copper foil using a mixture of NG, styrene–butadiene rubber (SBR), and carboxymethyl cellulose (CMC) at a weight ratio of 98:1:1. The areal loading was 5.5 mg cm^{-2}, and the electrode density after pressing was 1.45 g cm^{-3}. The thickness of the anode active material layer was approximately 48 μm.

Relatively thin electrodes were intentionally employed to minimize liquid-phase resistance and concentration polarization under high-rate conditions.

2.3. Pouch-type cells

The cathode and anode sheets described in Section 2.2 were assembled into pouch-type cells with a nominal capacity of 19 mAh. The cathode active area was 4 cm × 3 cm, and the cells were cathode-limited. The N/P ratio, defined as the ratio of the initial anode charge capacity to the initial cathode charge capacity, was approximately 1.3.

A 20 μm-thick trilayer polypropylene/polyethylene/polypropylene (PP/PE/PP) separator (Ube Maxell Co., Ltd., Japan) was placed between the electrodes. After electrolyte injection (1.0 mL per cell), the cells were vacuum-sealed under approximately 85% vacuum and subjected to a formation cycle to ensure electrolyte wetting and gas removal.

The formation protocol consisted of charging to 4.2 V under constant-current/constant-voltage (CCCV) mode, followed by discharging to 3.0 V under constant-current (CC) mode at 1C (based on nominal capacity). After the initial formation cycle, the cells were opened, degassed, and resealed under reduced pressure.

2.4. Symmetric cells

At 50% state of charge (SOC), pouch cells were disassembled in an argon-filled glove box, and both electrodes were rinsed twice with DMC. Electrode laminate sheets (3 cm × 4 cm) were punched from the central region into disks. The NCM523 cathode was punched into 14 mm diameter disks, and the NG anode was punched into 15 mm diameter disks.

To separately evaluate cathode and anode impedance, symmetric NCM523/NCM523 and NG/NG CR2032 coin cells were assembled according to a previously reported procedure [14]. A 20 μm-thick trilayer PP/PE/PP separator (19 mm diameter) was placed between identical electrodes. A glass fiber separator (Whatman GF/A, Cytiva; 16 mm diameter) was additionally inserted to improve electrolyte retention.

Approximately 0.2 mL of electrolyte (1 M $LiPF_6$ in EC/DMC = 1:2 (v/v) with 2.5 wt% VC) was added prior to cell assembly.

Symmetric cells were prepared from pouch cells harvested after the 6th and 301st cycles. Because the samples originated from different pouch cells, slight variations in impedance values may be present. Therefore, the reported values represent the average of two independently prepared cells.

2.5. Cycling performance and impedance evaluation

Galvanostatic charge–discharge tests of pouch cells were performed using an ACD-M02C battery testing system with an AC impedance measurement option (ASKA Electronic Co., Ltd., Japan) at 25 °C and a 1C rate (1C = 19 mA).

Electrochemical impedance spectroscopy (EIS) measurements for symmetric NCM523/NCM523 and NG/NG CR2032 coin cells were carried out using an SP-150 potentiostat (Bio-Logic Science Instruments, France) at 25 °C and 50% state of charge (SOC). An AC amplitude of 10 mV was applied over a frequency range from 500 kHz to 1 mHz.

The impedance of pouch cells was also measured under identical conditions, except that the frequency range was 200 kHz to 1 mHz.

All measurements were conducted using at least two independently prepared cells. Representative spectra are shown for clarity, and symmetric cell results are reported as averaged values to reduce cell-to-cell variation. The impedance spectra were fitted using ZView 4.1b software (Scribner Associates, Inc.) with the equivalent circuit models shown in Fig. S1, and the fitting parameters are summarized in Tables S1-S4.

2.6. Reductive decomposition potential

The reductive decomposition behavior was evaluated by cyclic voltammetry (CV) using an SP-150 potentiostat (Bio-Logic Science Instruments, France). A stainless steel mesh welded to a stainless steel plate was used as the current collector for the working electrode, onto which the NG electrode was attached.

A three-electrode beaker cell configuration (NG/Li/Li; working/counter/reference) was employed. Measurements were conducted at 25 °C at a scan rate of 0.1 mV s^{-1} over a potential range of 0.005–2.0 V vs. Li/Li^+. The baseline current fluctuation was within ±0.01 mA cm^{-2} under the present measurement conditions. Current responses within this range were regarded as baseline fluctuations rather than distinguishable additive-derived electrochemical features.

2.7. Oxidative decomposition potential

A typical conductive additive in NCM523 cathodes, AB, was employed as the working electrode according to the procedure reported in Ref. 15. Because AB is commonly used as a conductive additive in NCM523 cathodes and provides a high electrochemically active surface area, it facilitates detection of additive oxidation behavior. However, the oxidative response obtained with AB may not fully reproduce the behavior of practical NCM523 electrodes.

A slurry was prepared by mixing AB (DENKA BLACK Li-400, Denka Co., Ltd., Japan) with a 5 wt% PVdF solution in NMP (#9305, Kureha Corporation, Japan) at an AB:PVdF mass ratio of 70:30. The slurry was coated onto Al foil, dried at 70 °C, and roll-pressed. The electrode was then welded to a 0.5 mm-thick Al plate to serve as the AB working electrode. The total loading (AB + PVdF) was approximately 0.59 mg cm^{-2}, corresponding to 0.41 mg cm^{-2} of AB.

Linear sweep voltammetry (LSV) was performed using SP-150 potentiostat (Bio-Logic Science Instruments, France) in a three-electrode glass cell configuration (AB/Li/Li). Measurements were conducted at 25 °C by scanning from the open-circuit voltage (OCV) toward the anodic direction at 5 mV s^{-1} until the current reached 100 mA. The oxidative decomposition potential was defined as the potential at which the current density reached 0.4 mA g^{-1} (normalized to AB mass).

2.8. Electrode surface analysis

Scanning electron microscopy (SEM) and X-ray photoelectron spectroscopy (XPS) were used to analyze the cathode surface of NCM523 and the anode surface of graphite. Samples were obtained by disassembling full NCM523/NG cells after the fifth discharge cycle. Each electrode was rinsed twice with DMC to remove residual electrolyte and then dried. SEM observations were performed using a JSM-7001F (JEOL Ltd., Japan). XPS measurements were conducted using an ESCA 5600 (ULVAC-PHI, Japan).

The composition and thickness of the SEI were evaluated by XPS following a previously reported procedure [16]. Because the electrode surface is rough and porous, unetched regions may remain within pores during sputtering. Therefore, the apparent SEI thickness was defined as the sputtering depth at which the carbon atomic fraction (excluding lithium) reached 95%.

3. Results and discussion

3.1. Molecular structures of the investigated additives

Lithium methanesulfonate (CH_3SO_3Li), which was previously identified as a surface-related species in our earlier work [16], was investigated together with structurally related sulfonate- and sulfate-based lithium salts.

Fig. 1 shows the molecular structures of the investigated additives: (a) CH_3SO_3Li (low solubility), (b) FSO_3Li (high solubility), (c) CF_3SO_3Li (high solubility), (d) CH_3OSO_3Li (intermediate solubility), and (e) $C_2H_5OSO_3Li$ (intermediate solubility).

These compounds differ in substituent groups (–CH_3, –CF_3, –F, –C_2H_5), linkage structure (sulfonate vs. sulfate), and solubility in the present electrolyte system, providing a basis for comparing their effects on impedance evolution.

The solubility of each additive in 1 M $LiPF_6$ in EC/DMC (1:2 v/v) containing 2.5 wt% VC was estimated at room temperature by visual inspection. The additives were added incrementally to the electrolyte under stirring, and the highest concentration at which no visible undissolved solid remained was taken as the approximate solubility limit. The obtained values were used to classify the additives into low-, intermediate-, and high-solubility categories.

3.2. Cycle performance of NCM/NG pouch cells

The influence of the additives on cycling behavior was evaluated using NCM523/NG pouch cells. The apparent solubility limits of the additives in 1 M $LiPF_6$ in EC/DMC (1:2 v/v) containing 2.5 wt% VC were estimated to be <0.1 wt% for (a), ~0.5 wt% for (d), and ~2 wt% for (e). These concentrations were selected to ensure complete dissolution under the present test conditions. Additives (b) and (c), which exhibited high solubility (>20 wt%) in the base electrolyte, were evaluated at 1 wt % (Table 1). This concentration was selected as a practical level that ensured complete dissolution while minimizing potential side reactions, including Al current collector corrosion during extended cycling.

Fig. 2 shows the cycling performance of the pouch cells containing each additive. Under 1 C cycling at 25 °C, all cells exhibited highly similar capacity retention over 300 cycles, indicating that the incorporation of sulfonate- and sulfate-based lithium salts does not adversely affect long-term cycling stability within the investigated concentration range.

The similar capacity retention observed for all cells provides a stable basis for evaluating impedance evolution independently of capacity fade. Therefore, the differences discussed in Sections 3.3–3.5 are attributed primarily to interfacial phenomena rather than bulk degradation.

3.3. Electrode impedance analysis using symmetric cells

Symmetric cells were employed to separately evaluate impedance contributions from the anode and cathode. Hereafter, “no additive” refers to the baseline electrolyte containing 2.5 wt% VC as the sole additive.

Because symmetric cells consist of two identical electrodes, the measured impedance represents the combined response of both electrodes. After subtraction of the bulk electrolyte impedance, the remaining impedance was divided by two to estimate single-electrode behavior.

At the anode, impedance values remained relatively stable during cycling. For the baseline electrolyte, the anode impedance was 3.3 Ω at the 6th cycle and 3.8 Ω at the 301st cycle (Fig. 3). Similar trends were observed for all additives, suggesting that anode processes contribute only marginally to overall impedance evolution.

In contrast, cathode impedance showed a significant increase during

Table 1
Estimated additive solubility and pouch cell cycling performance.

Additive	Estimated solubility	300th/5th (%)	300th CE (%)
Ref. (VC only)	-	94.64	99.90
CH_3SO_3Li	<0.1 wt%	95.40	99.86
CH_3OSO_3Li	~0.5 wt%	96.95	99.89
$C_2H_5OSO_3Li$	~2 wt%	98.98	99.83
FSO_3Li	>20 wt%	94.40	99.91
CF_3SO_3Li	>20 wt%	93.75	99.82

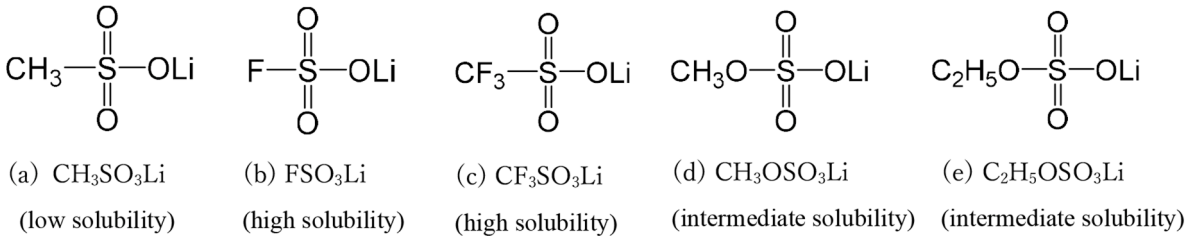

Fig. 1. Chemical structures of the investigated additives.

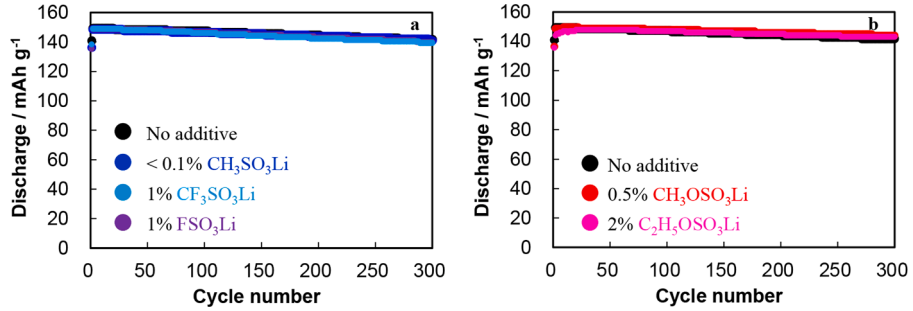

Fig. 2. Cycling performance of NCM/NG pouch cells using 1 M $LiPF_6$ in EC/DMC (1:2) with 2.5 wt% VC and additive at 25 °C.

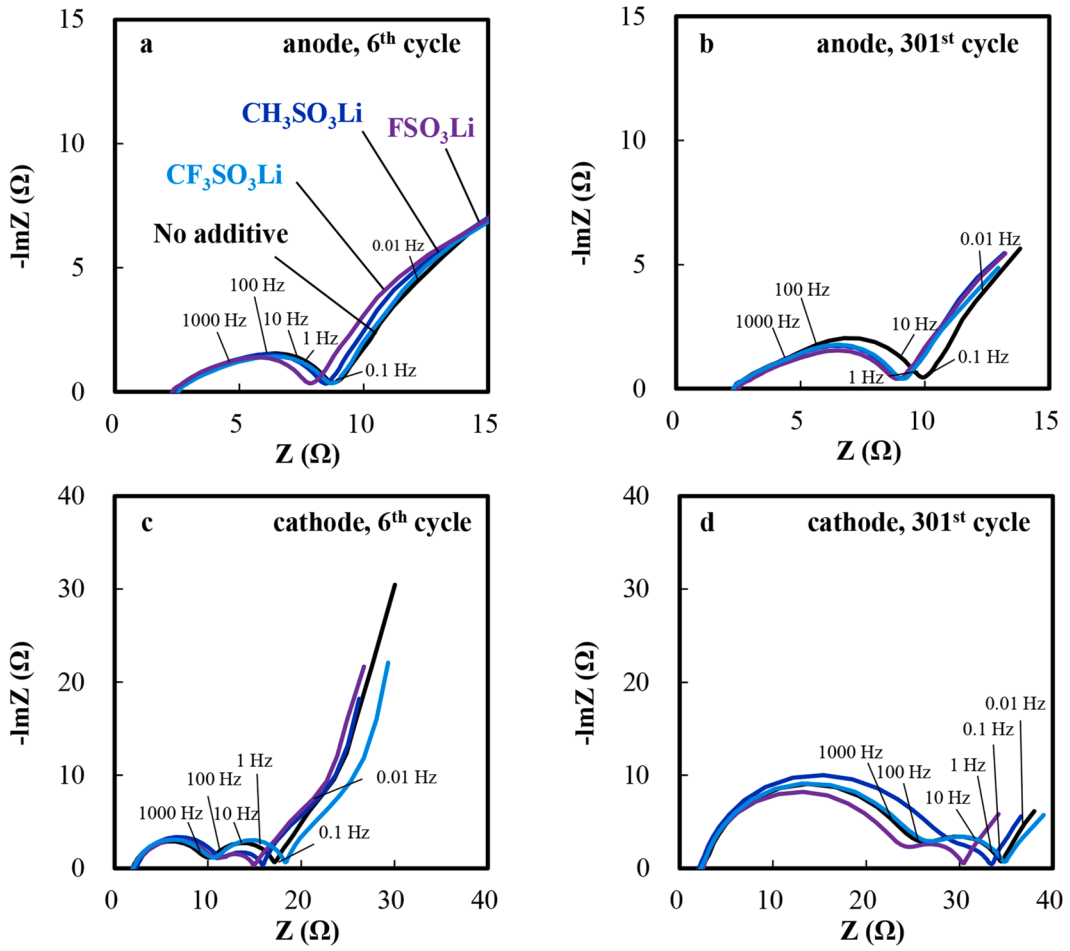

Fig. 3. Impedance spectra at 25 °C of NG/NG (a,b,e,f) and NCM523/NCM523 (c,d,g,h) symmetric cells. (a–d) CH_3SO_3Li, FSO_3Li, and CF_3SO_3Li; (e–h) CH_3OSO_3Li and $C_2H_5OSO_3Li$. (i, j) NCM523/NG full cells with CH_3SO_3Li, FSO_3Li, and CF_3SO_3Li; (k, l) full cells with CH_3OSO_3Li and $C_2H_5OSO_3Li$. Panels (a, c, e, g, i, k) show the 6th cycle, and (b, d, f, h, j, l) show the 301st cycle.

cycling. For the baseline electrolyte, it increased from 7.7 Ω to 16.5 Ω (6^{th} to 301^{st} cycle). Among RSO_3Li additives, CH_3SO_3Li and FSO_3Li showed moderate suppression of impedance growth, whereas CF_3SO_3Li exhibited behavior similar to the baseline. $ROSO_3Li$ additives exhibited smaller impedance increases, particularly CH_3OSO_3Li (5.8 → 12.4 Ω), followed by $C_2H_5OSO_3Li$ (6.1 → 13.2 Ω). These results suggest that impedance evolution under the present conditions is primarily influenced by cathode-side processes.

The high-frequency intercept showed negligible variation across all systems, indicating that the bulk electrolyte impedance remained essentially constant. Thus, the differences in impedance are attributed primarily to interfacial processes rather than changes in ionic conductivity, consistent with the similar R_o values listed in Tables S1–S4.

Total cell impedance reduction followed the order: CH_3OSO_3Li (~30%) > $C_2H_5OSO_3Li$ (~24%) > FSO_3Li (~17%) > CH_3SO_3Li (minor change) > CF_3SO_3Li (slight increase ~6%), relative to the baseline electrolyte (Fig. 4).

Impedance spectra of both symmetric and full cells exhibited a mid-frequency semicircle (10^2–10° Hz), commonly associated with interfacial charge-transfer resistance. The growth of this feature during cycling was significantly suppressed in $ROSO_3Li$-containing systems, while the high-frequency intercept remained unchanged. These results indicate

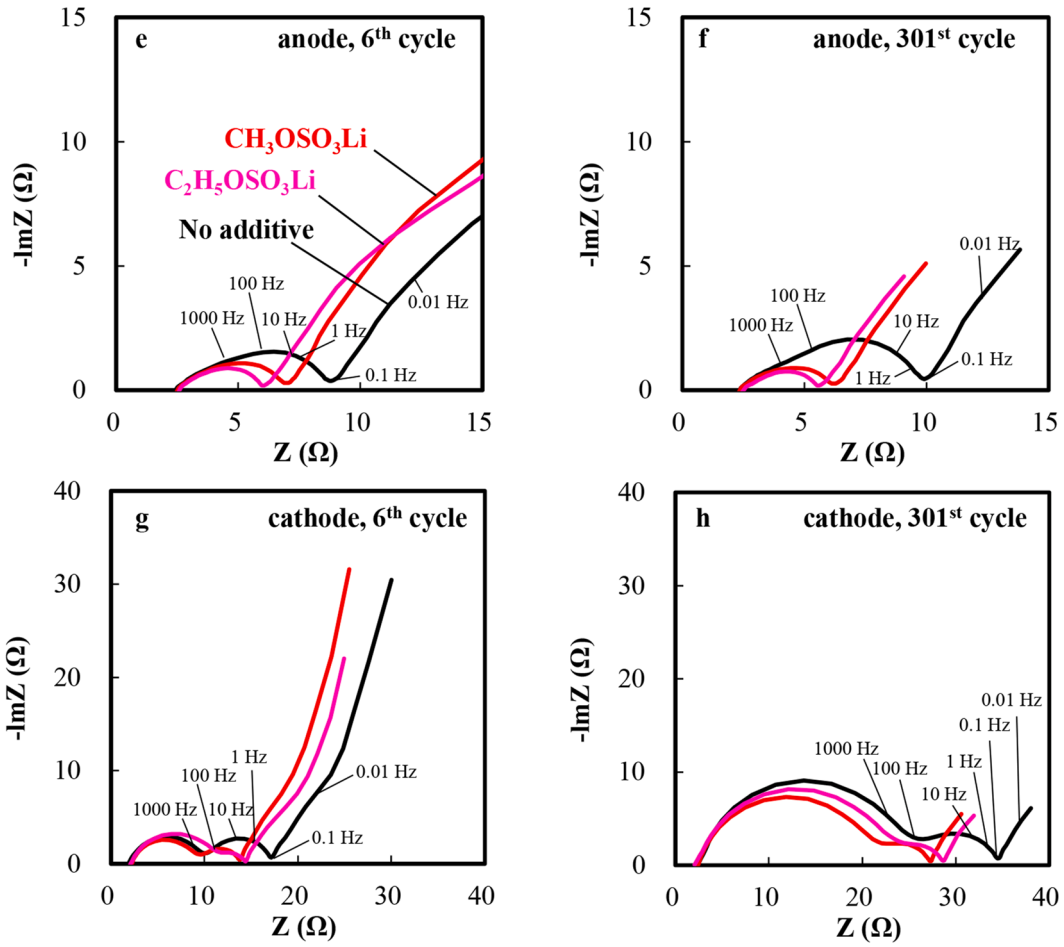

Fig. 3. (*continued*).

that the observed impedance reduction is primarily associated with suppression of cathode interfacial impedance growth.

3.4. Electrochemical stability of additives

To examine whether the observed impedance reduction is associated with electrochemical reactions of the additives, their oxidative and reductive stability was evaluated by linear sweep voltammetry (LSV) and cyclic voltammetry (CV), respectively (Fig. 5), using 1 M $LiPF_6$ in EC/DMC (1:2 v/v) as the supporting electrolyte.

The oxidative current profiles obtained using the AB working electrode (Fig. 5, upper panel) were essentially unchanged by additive addition, and no additional oxidation features were observed in the cathode operating range.

In the reduction region using the NG working electrode (Fig. 5, lower panel), only minor shifts in peak position were observed, while the reduction onset and inflection potentials (approximately 0.9 V vs. Li/Li^+) remained essentially unchanged across all samples. These features are attributed mainly to EC reductive decomposition rather than additive-derived processes. The observed current responses remained within the baseline fluctuation range (± 0.01 mA cm^{-2}), and no distinguishable additive-derived peaks were detected.

Overall, no distinguishable redox signatures attributable to the additives were detected in either CV or LSV. These results suggest that the additives do not undergo significant sacrificial oxidation or reduction under the present conditions. Accordingly, the observed impedance reduction is more reasonably associated with interfacial modification processes rather than a dominant redox decomposition pathway.

3.5. SEM analysis of electrode surfaces

Because LSV and CV measurements did not show distinct electrochemical decomposition features of the additives (Section 3.4), SEM was performed to examine possible morphological changes on both electrodes after cycling (Fig. 6).

On the anode, the baseline (no-additive) sample exhibited relatively small and localized surface features. In the presence of CH_3OSO_3Li and CH_3SO_3Li, more widely distributed surface features were observed (Fig. 6, upper panel). However, CH_3SO_3Li showed only minor changes in anode impedance (Section 3.3), suggesting that the observed morphological differences are not directly correlated with the impedance behavior. No major morphological differences were detectable by SEM, although the presence of ultrathin interfacial layers below the spatial resolution of SEM cannot be excluded.

On the cathode, no clear morphological differences were observed among the baseline, CH_3OSO_3Li-, and CH_3SO_3Li-containing samples (Fig. 6, lower panel). The small particles observed locally are attributed to binder or conductive carbon residues rather than additive-derived species. The absence of distinguishable morphological changes is consistent with the formation of a thin CEI below the spatial resolution of SEM.

3.6. XPS analysis of electrode surfaces

Because SEM observations did not provide clear evidence of additive-derived surface deposits (Fig. 6), XPS was performed to analyze the surface chemistry of both electrodes after cycling (Fig. 7).

Depth profiling of graphite electrodes revealed no significant

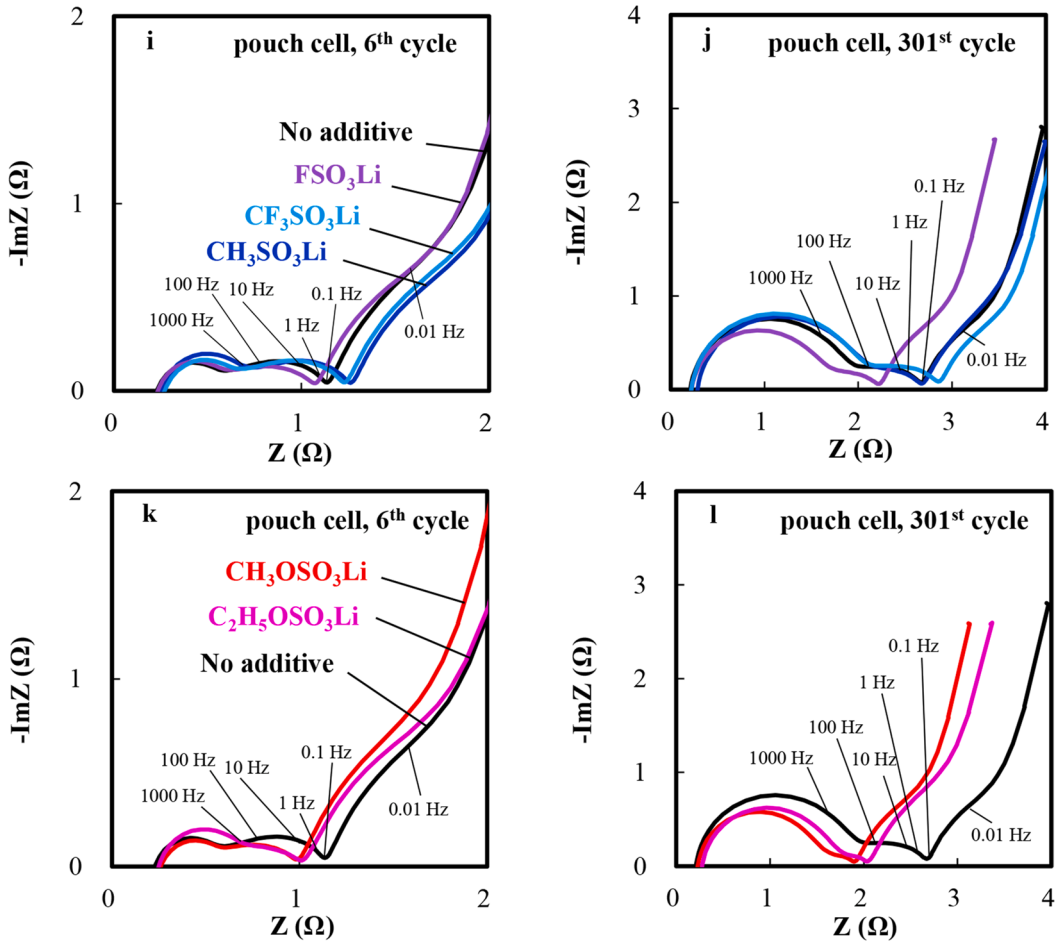

Fig. 3. (*continued*).

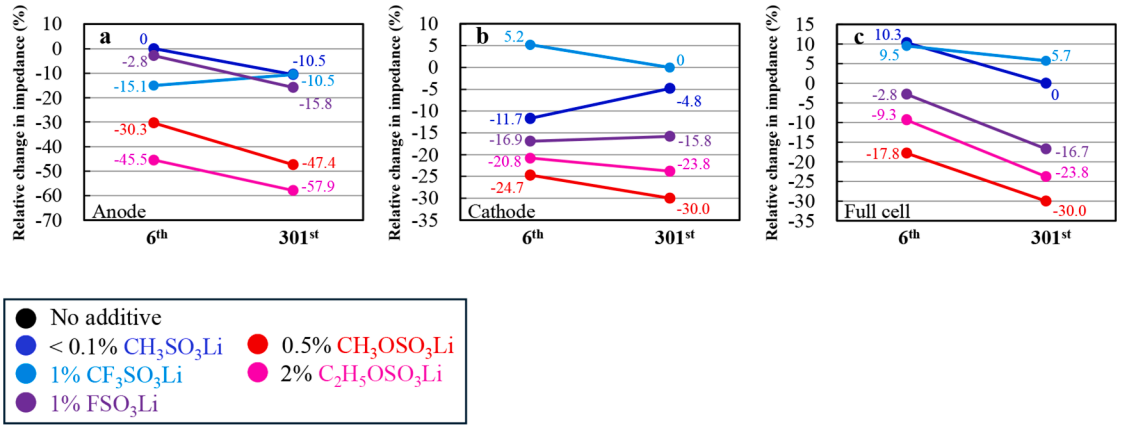

Fig. 4. Comparison of impedance spectra at 25 °C for (a) NG/NG, (b) NCM523/NCM523, and (c) NCM523/NG cells. Impedance reduction rates are shown relative to the baseline electrolyte (No additive = VC only).

differences in apparent SEI thickness among the baseline, CH_3OSO_3Li-, and CH_3SO_3Li-containing systems within the experimental resolution (Fig. 7a–c), suggesting that SEI thickness is not the dominant factor governing impedance differences. Consistent with this observation, XPS depth profiles of the NG electrodes (Fig. S2) showed similar elemental distributions for the VC-only, CH_3OSO_3Li, and CH_3SO_3Li systems, supporting that the apparent interphase thickness was not substantially altered by the additives.

In the F 1 s spectra, a peak at approximately 685 eV corresponding to LiF was observed for the baseline (VC-containing) and CH_3SO_3Li systems, whereas reduced LiF intensity was observed for CH_3OSO_3Li (Fig. 7d). The C 1 s, Li 1 s, and O 1 s spectra showed similar features across all samples, attributed to ($ROCO_2Li$), Li_2CO_3, and related inorganic species (Fig. 7e–g).

In contrast, S 2p signals at approximately 170 eV, assigned to sulfate/sulfonate-derived species, were detected exclusively in the additive-containing systems (Fig. 7h). These results indicate the presence of sulfur-containing species in the SEI without a substantial increase in

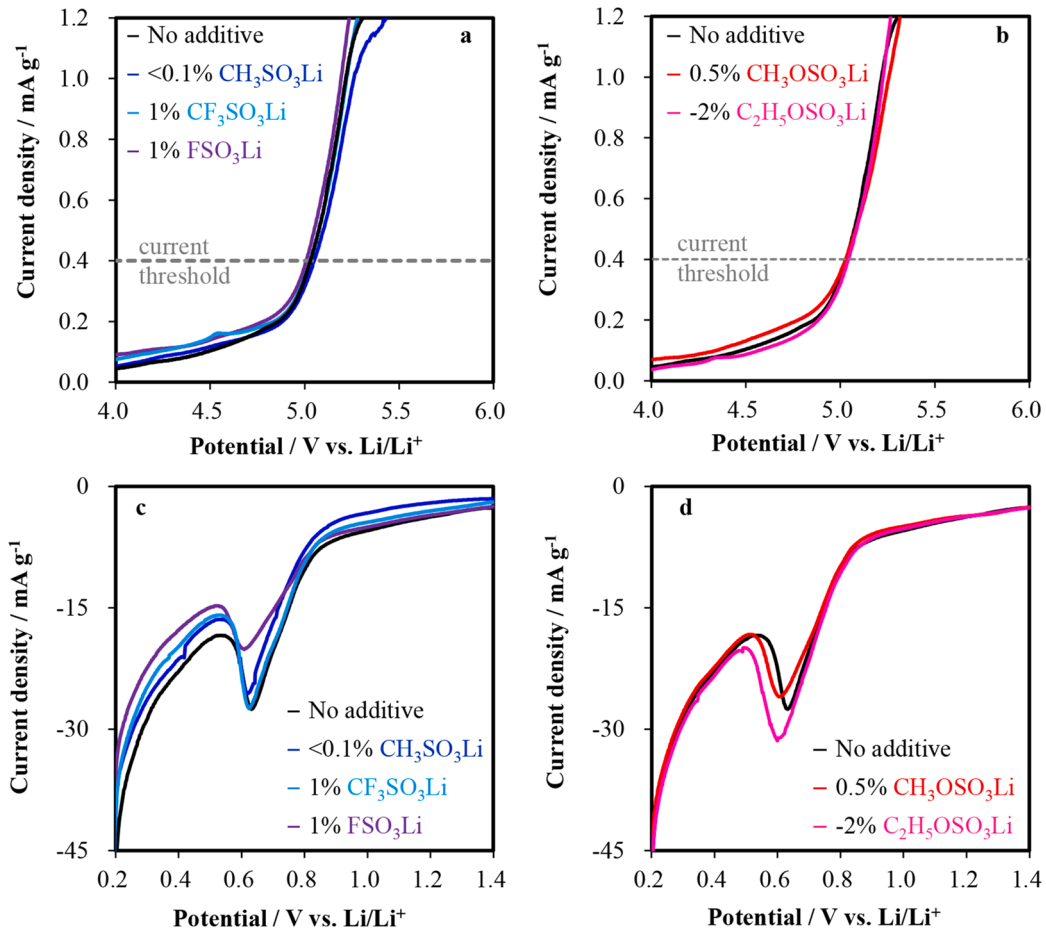

Fig. 5. Electrochemical stability of 1 M $LiPF_6$ in EC/DMC (1:2, v/v) containing additives, evaluated by LSV (upper, working electrode: AB; counter/reference: Li/Li^+) and CV (lower, working electrode: NG; counter/reference: Li/Li^+).

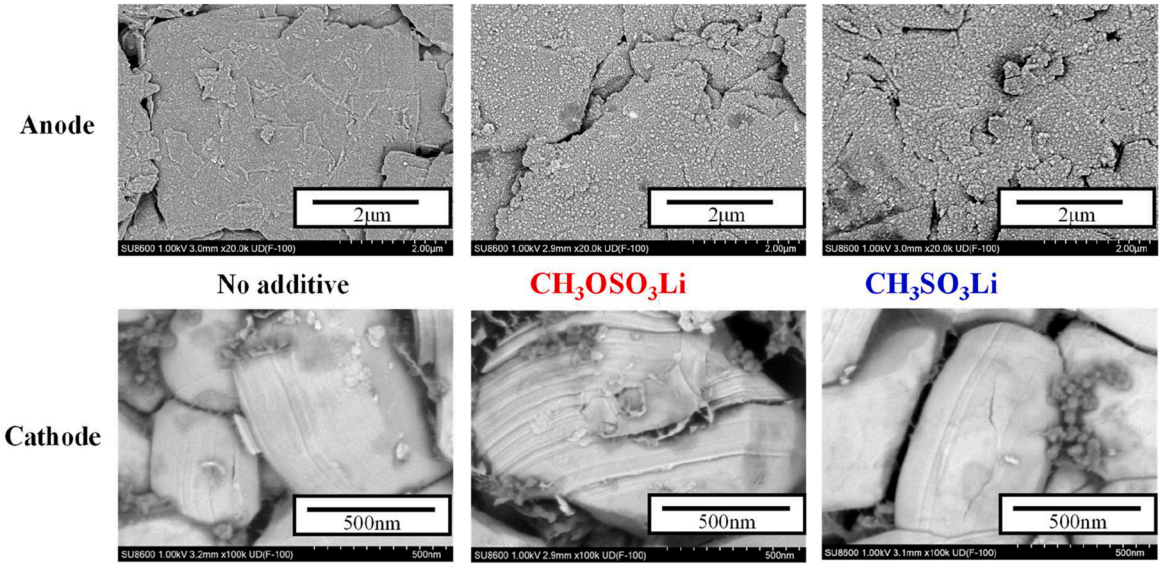

Fig. 6. SEM images (backscattered electron mode) of electrodes after cycling. Upper: anode; lower: cathode.

interphase thickness. The greater impedance suppression observed for CH_3OSO_3Li may therefore be related to differences in the distribution and/or chemical environment of sulfur-containing species, rather than SEI thickness.

For NCM523 cathodes, no pronounced differences were observed in the F 1 s, C 1 s, Li 1 s, or O 1 s spectra among the samples (Fig. 7i–l). S 2p signals at approximately 170 eV were again detected in the additive-containing systems (Fig. 7m), while a weak background signal was also present in the baseline electrolyte.

This background sulfur is attributed to residual sulfate species

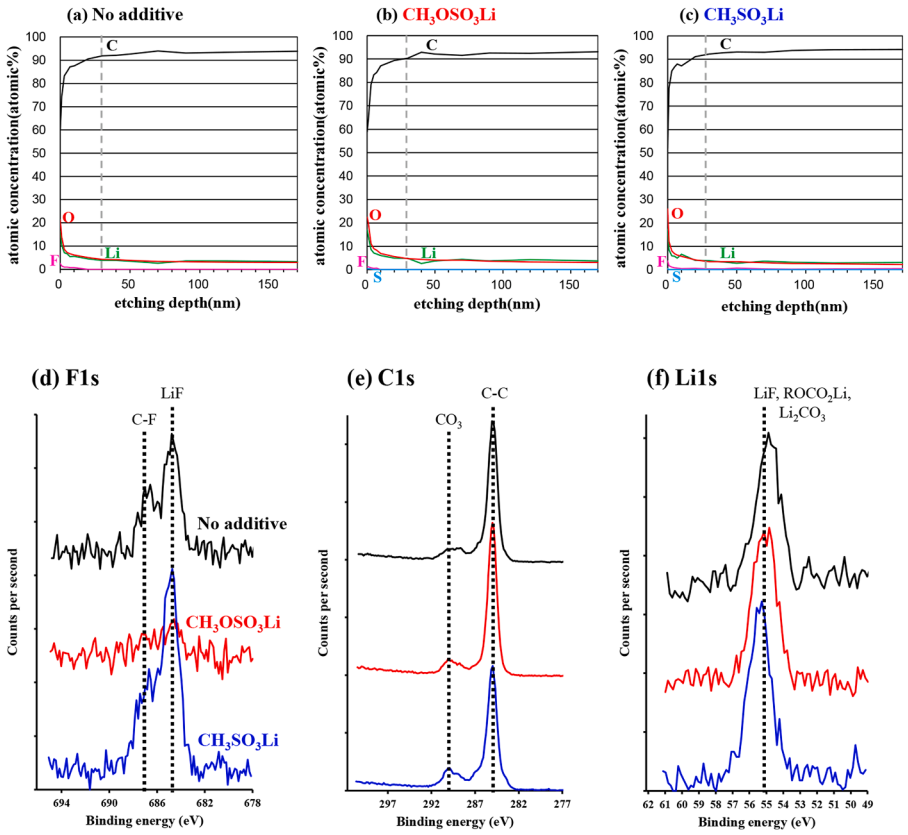

Fig. 7. XPS depth profiles of NG electrodes (a–c). XPS spectra of NG (d–h) and NCM523 (i–m): F 1 s, C 1 s, Li 1 s, O 1 s, and S 2p, corresponding to the baseline electrolyte (VC only), CH_3OSO_3Li, and CH_3SO_3Li, respectively.

originating from the coprecipitation synthesis of the NCM precursor (e.g., $NiSO_4$, $CoSO_4$, and $MnSO_4$) [17]. The increased S 2p intensity in the additive-containing samples suggests enrichment of sulfur-containing species in the CEI. SEM did not reveal clear morphological changes, and the detection of transition-metal signals (Ni, Co, Mn) at the outermost surface suggests that the CEI is thin and within the effective probing depth of XPS rather than forming a thick surface layer.

3.7. *Interfacial origin of impedance reduction*

The SEI composition is discussed based on established models reported previously [18–21], while the CEI structure is considered in accordance with reported models for layered oxide cathodes [22]. Typical CEI components such as LiF and $Li_xPO_yF_z$ have been widely reported in the literature [23–26].

The absence of distinct oxidative or reductive features in CV and LSV measurements suggests that CH_3SO_3Li and CH_3OSO_3Li do not undergo significant electrochemical decomposition within the investigated voltage window. Accordingly, sulfur-containing species detected by XPS are attributed to sulfonate- or sulfate-derived species incorporated into the interphase. Minor chemical transformations below the detection limit cannot be completely excluded.

A dependence of impedance evolution on additive solubility was observed. Sparingly soluble additives (<0.1 wt%) are unlikely to provide sufficient interfacial availability, whereas highly soluble salts (>20 wt%) are expected to remain predominantly in the bulk electrolyte. In contrast, additives with intermediate solubility (0.5–2 wt%) consistently exhibited the most effective suppression of charge-transfer resistance growth.

These results are consistent with a scenario in which moderately soluble sulfate species may be preferentially distributed near the electrode/electrolyte interface. Although direct structural evidence of molecular arrangement at the interface is not available, the consistency across electrochemical, impedance, and surface analyses suggests that the interfacial distribution of sulfate-related species is an important factor associated with impedance suppression, rather than conventional sacrificial decomposition pathways (Fig. 8). Further investigations of solvation structure (e.g., Raman spectroscopy) and interfacial dynamics (e.g., in situ EIS) would provide direct validation of this interpretation. It should be noted that the present results do not provide a complete spectroscopic comparison across the entire solubility range, and the proposed interfacial enrichment interpretation should therefore be regarded as a working model requiring further validation.

Recent studies have attributed the effects of electrolyte additives mainly to interphase formation and its influence on electrochemical performance [27,28]. In contrast, the present study examines a series of sulfur-containing lithium salts and suggests that additive solubility may be associated with impedance evolution and suppression of charge-transfer resistance growth during cycling. Although the underlying mechanism remains to be clarified, these findings provide a complementary perspective to conventional interphase-based interpretations and indicate that additive solubility may represent an additional factor influencing interfacial impedance evolution.

Because all measurements were conducted at a fixed E/C ratio, the influence of electrolyte loading on additive availability and interfacial behavior was not investigated in the present study. Furthermore, the observed relationship between additive solubility and impedance evolution was established only under the electrolyte loading conditions employed here and should not be directly generalized to practical low-E/C cells without further validation.

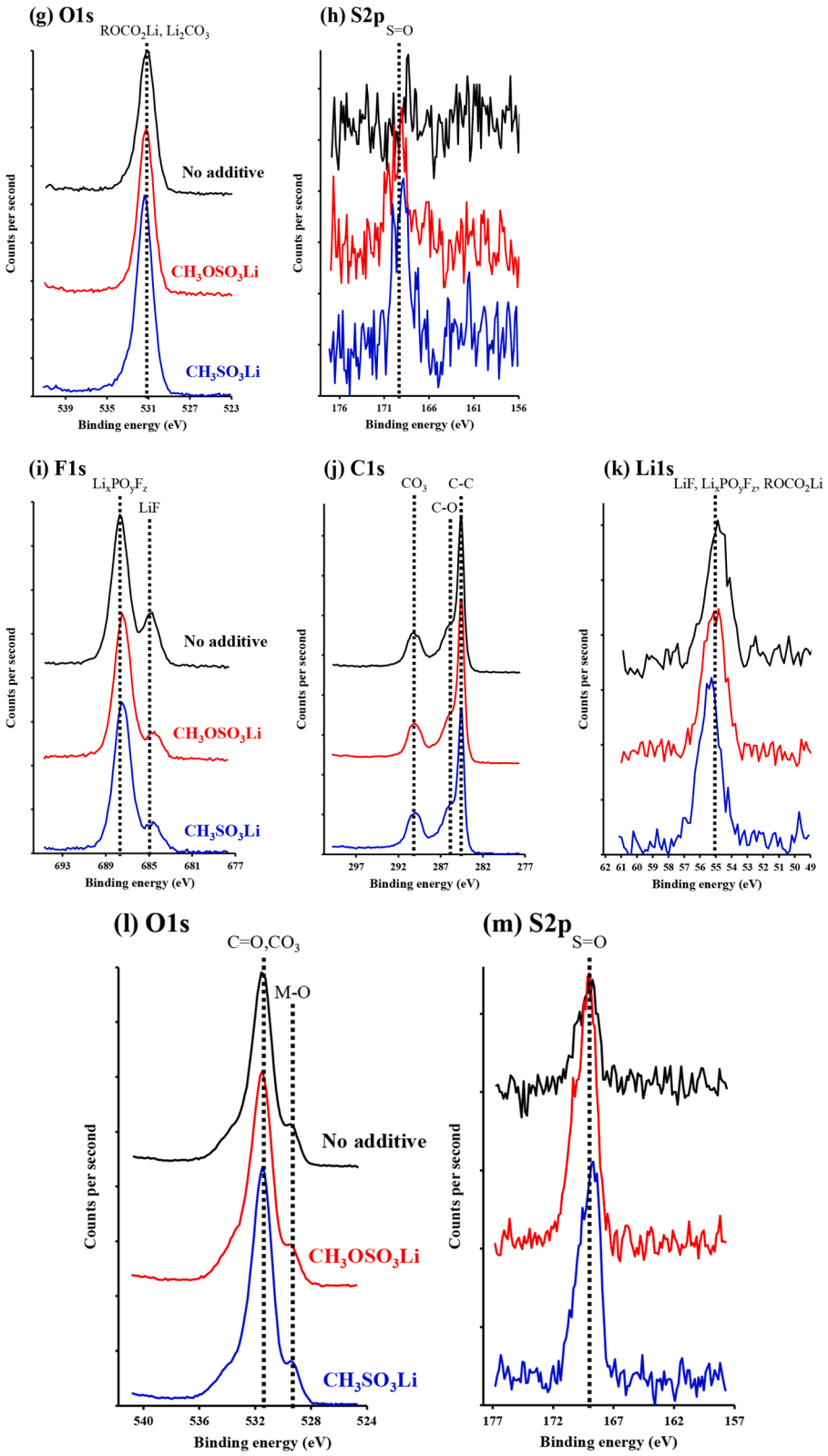

Fig. 7. (*continued*).

4. Conclusion

Lithium salts containing sulfonate and sulfate functional groups were comparatively investigated as electrolyte additives for impedance control in NCM523/NG pouch cells operated under practical 1 C cycling conditions. Among the additives examined, ROSO3Li-type additives, particularly CH_3OSO_3Li, exhibited the most effective suppression of cathode impedance growth compared with the baseline electrolyte, while maintaining stable capacity retention for over 300 cycles. Full-cell impedance measurements showed up to a 30% decrease in total cell impedance after 300 cycles at 25 °C relative to the VC-containing baseline electrolyte.

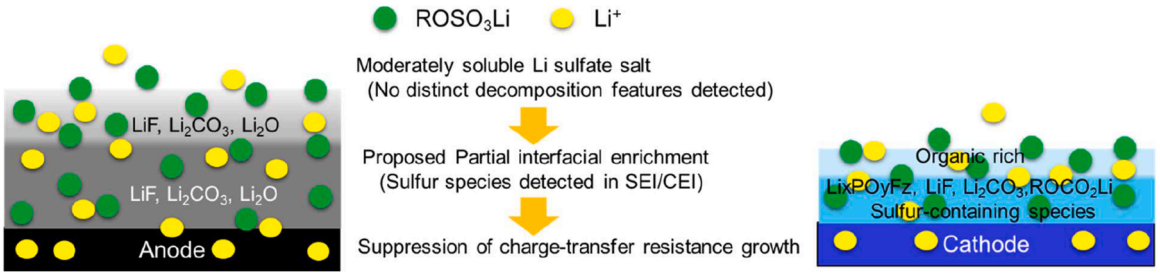

Fig. 8. Schematic illustration of a working model for suppression of charge-transfer resistance growth by moderately soluble lithium sulfate additives.

Electrochemical measurements revealed no distinct additive-derived redox features within the investigated voltage window. SEM analysis showed no significant morphological differences correlated with impedance evolution. In contrast, XPS depth profiling confirmed the presence of sulfur-containing species at both cathode and anode surfaces in the additive-containing systems, although no measurable increase in the apparent interphase thickness was observed. These results indicate that sulfur-containing species are incorporated into the interphase without formation of a thick decomposition-derived layer.

Impedance suppression was found to be associated with additive solubility under the conditions investigated in this study. Low solubility (<0.1 wt%) likely limits interfacial availability, whereas excessively high solubility (>20 wt%) may reduce effective interfacial participation due to preferential retention in the bulk electrolyte. In contrast, moderate solubility (0.5–2 wt%) appears to provide conditions favorable for interfacial modification.

Overall, the combined electrochemical and surface analytical results are consistent with an interfacial-enrichment interpretation rather than a conventional sacrificial decomposition pathway. The present findings suggest that additive solubility may represent an important parameter influencing interfacial behavior in LIB electrolytes. Further in situ spectroscopic studies and solvation structure analysis would be valuable for direct investigation of the proposed interfacial behavior.

CRediT authorship contribution statement

Koji Abe: Writing – review & editing, Writing – original draft, Supervision, Resources, Project administration, Investigation, Funding acquisition, Conceptualization. **Keitatsu Miura:** Visualization, Validation, Methodology, Investigation, Formal analysis, Data curation. **Yanko Marinov Todorov:** Writing – review & editing, Visualization, Validation, Methodology, Investigation, Formal analysis, Data curation, Conceptualization. **Masaki Deguchi:** Writing – review & editing, Validation, Methodology, Investigation, Formal analysis, Data curation, Conceptualization.

Declaration of competing interest

The authors declare that they have no known competing financial interests or personal relationships that could have appeared to influence the work reported in this paper.

Supplementary materials

Supplementary material associated with this article can be found, in the online version, at doi:10.1016/j.electacta.2026.149342.

Data availability

Data will be made available on request.

References

[1] T. Fukutsuka, K. Koyamada, S. Maruyama, K. Miyazaki, T. Abe, Electrochim. Acta 199 (2016) 380, https://doi.org/10.1016/j.electacta.2016.03.049.
[2] N. Ogihara, S. Kawauchi, C. Okuda, Y. Itou, Y. Takeuchi, Y. Ukyo, J. Electrochem. Soc. 159 (7) (2012) A1034, https://doi.org/10.1149/2.057207jes.
[3] H. Yoshitake, Battery and Power Supply. Techno-Frontier Symposium, Japan Management Associates Makuhari, 1999. Paper F5-3.
[4] K. Abe, H. Yoshitake, Electrochemistry 72 (2004) 520, https://doi.org/10.5796/electrochemistry.72.519.
[5] K. Abe, Nonaqueous electrolytes and advances in additives, in: T.R. Jow, K. Xu, O. Borodin, M. Ue (Eds.), Electrolytes For Lithium and Lithium-ion Batteries, Modern Aspects of Electrochemistry, 58, Springer, New York, 2014, pp. 167–225, https://doi.org/10.1007/978-1-4939-0302-3_3.
[6] A.M. Haregewoin, A.S. Wotango, B.-J. Hwang, Energy Environ. Sci. 9 (2014) 1955, https://doi.org/10.1039/C6EE00123H.
[7] K. Xu, Chem. Rev. 114 (2014) 11503, https://doi.org/10.1021/cr500003w.
[8] H. Ota, Y. Sakata, A. Inoue, S. Yamaguchi, J. Electrochem. Soc. 151 (2004) A1659, https://doi.org/10.1149/1.1785795.
[9] P. Verma, P. Maire, P. Novák, Electrochim. Acta 55 (2010) 6332, https://doi.org/10.1016/j.electacta.2010.05.072.
[10] S.J. An, J. Li, C. Daniel, D. Mohanty, S. Nagpure, D.L. Wood III, Carbon 105 (2016) 52, https://doi.org/10.1016/j.carbon.2016.04.008.
[11] Y. Hai, T. Tran, K. An, D.T.T. Vu, S.W. Song, ACS Energy Lett. 10 (2025) 356, https://doi.org/10.1021/acsenergylett.4c02860.
[12] X. Shi, T. Zheng, J. Xiong, B. Zhu, Y.-J. Cheng, Y. Xia, ACS Appl. Mater. Interfaces 13 (2021) 57107, https://doi.org/10.1021/acsami.1c15690.
[13] T. Kim, L.K. Ono, Y. Qi, J. Mater. Chem. A 11 (2023) 221, https://doi.org/10.1039/d2ta07565b.
[14] K. Abe, M. Colera, K. Shimamoto, M. Kondo, K. Miyoshi, J. Electrochem. Soc. 161 (2014) A863, https://doi.org/10.1149/2.086405jes.
[15] Z. Zhang, J. Hu, Y. Hu, H. Wang, H. Hu, J. Colloid Interface Sci. 669 (2024) 305, https://doi.org/10.1016/j.jcis.2024.05.009.
[16] K. Miura, M. Deguchi, Y.M. Todorov, K. Abe, Electrochim. Acta 539 (2025) 147054, https://doi.org/10.1016/j.electacta.2025.147054.
[17] L. Liang, K. Du, Z. Peng, Y. Cao, J. Duan, J. Jiang, G. Hu, Electrochim. Acta 130 (2014) 82, https://doi.org/10.1016/j.electacta.2014.02.100.
[18] E. Peled, D. Golodnitsky, G. Ardel, J. Electrochem. Soc. 144 (1997) L208, https://doi.org/10.1149/1.1837858.
[19] S. Park, S. Kim, J. Lee, M. Ue, N. Choi, Chem. Sci. 14 (2023) 9996, https://doi.org/10.1039/d3sc03514j.
[20] S. Heiskanen, J. Kim, B.L. Lucht, Joule 3 (2019) 2322, https://doi.org/10.1016/j.joule.2019.08.018.
[21] V.A. Agubra, J.W. Fergus, J. Power Sources. 268 (2014) 153, https://doi.org/10.1016/j.jpowsour.2014.06.024.
[22] N. Zhang, B. Wang, F. Jin, Y. Chen, Y. Jiang, C. Bao, J. Tian, J. Wang, R. Xu, Y. Li, Q. Lv, H. Ren, D. Wang, H. Liu, S. Dou, X. Hong, Cell Rep. Phys. Sci. 3 (2022) 101197, https://doi.org/10.1016/j.xcrp.2022.101197.
[23] J. Wu, Nano Micro Lett. 14 (2022) 166, https://doi.org/10.1007/s40820-022-00917-2.
[24] W. Liu, J. Li, W. Li, H. Xu, C. Zhang, X. Qiu, Nat. Commun. 11 (2020) 3629, https://doi.org/10.1038/s41467-020-17396-x.
[25] T. Eriksson, A.M. Andersson, C. Gejke, T. Gustafsson, J.O. Thomas, Langmuir 18 (2002) 3609, https://doi.org/10.1021/la011354m.
[26] J.N. Zhang, Q. Li, Y. Wang, J. Zheng, X. Yu, H. Li, Energy Storage Mater. 14 (2018) 1–7, https://doi.org/10.1016/j.ensm.2018.02.016.
[27] S. Luo, C. Ge, L. Ou, F. Zeng, Y. Wang, H. Lu, Electrochim. Acta 498 (2024) 144684, https://doi.org/10.1016/j.electacta.2024.144684.
[28] J. Lee, Y.K. Han, Electrochim. Acta 513 (2025) 145628, https://doi.org/10.1016/j.electacta.2024.145628.